# Numerical study of electron cyclotron drift instability in Hall thruster

**IEPC-2019-720**

*Presented at the 36th International Electric Propulsion Conference*
*University of Vienna • Vienna, Austria*
*September 15-20, 2019*

F. Taccogna[1] and P. Minelli[2]
*Institute for Plasma Science and Technology CNR, Bari, 70126, Italy*

**We study the cross-field electron transport in Hall thruster induced by ExB cyclotron drift instability. The investigation tool, consisting of one-dimensional Particle-in-Cell model in the azimuthal drift direction, has been subjected to a convergence study to verify the effects of numerical parameters. The instability evolves keeping the discrete nature of its cyclotron harmonics only for low wavenumbers. A resonance broadening mechanism induced by the electron heating and velocity distribution deformation makes the high-wave numbers disappear in the long non-linear stage. A large wavelength modulation, comparable to the entire azimuthal domain considered is always superimposed. The saturation mechanism is conducted by ions that, due to friction with electrons and trapping in the potential well, heat up and rotate along the electron drift direction. With the best numerical parameters found, the scaling of anomalous mobility with the most important physical quantities (gas and plasma density, magnetic field, accelerating axial electric field and ion mass) has been obtained. Results show that the electron cross-field mobility has a strong dependence from the plasma density and ion mass: for large plasma density, the system undergoes an abrupt change entering in a mode dominated by fluctuation-induced transport, while lighter ions present larger mobility.**

## Nomenclature

| | | |
|---|---|---|
| $B$ | = | magnetic field |
| $E$ | = | electric field |
| $f_{ei}$ | = | electron-ion friction force density |
| $k$ | = | wavenumber |
| $L_y$ | = | azimuthal length |
| $L_{z,acc}$ | = | acceleration region length |
| $m_e$ | = | electron mass |
| $M$ | = | ion mass |
| $N_g$ | = | number of grid points |
| $N_{ppc}$ | = | number of particles per cell |
| $N_p$ | = | total number of particles |
| $n$ | = | density |
| $q$ | = | elementary charge |
| $T$ | = | temperature |
| $u_E$ | = | electrostatic potential energy density |
| $v_{th,e}$ | = | electron thermal velocity |
| $v_{de}$ | = | electron ExB drift velocity |

[1] Researcher, Institute for Plasma Science and Technology CNR, francesco.taccogna@cnr.it.
[2] Researcher, Institute for Plasma Science and Technology CNR, pierpaolo.minelli@cnr.it.

$\beta$ = Hall parameter
$\Delta y$ = cell size
$\Delta t$ = time step
$\lambda$ = wavelength
$\lambda_{De}$ = electron Debye length
$\mu$ = mobility
$\omega$ = frequency
$\omega_{pe}$ = electron plasma frequency
$\omega_{pi}$ = ion plasma frequency
$\omega_{ce}$ = electron cyclotron frequency
$\nu_m$ = electron collisional frequency
$\rho_e$ = electron gyroradius

## I. Introduction

MEASURED electron cross-field mobility in Hall thrusters[1-4] results hundreds times larger than its classical collisional-induced value

$$\mu_{cl} = \frac{\frac{|q|}{m_e \nu_m}}{1+\frac{\omega_{ce}^2}{\nu_m^2}}. \tag{1}$$

Among the different mechanisms proposed[5-9] to explain the electron anomalous transport, the most plausible candidate is the electron ExB drift instability[10,11] generated by the unbalanced electron Hall current. It results in azimuthal modulations of electron/ion density and azimuthal electric field whose frequency and wavelength of the order of MHz and mm, respectively, have been observed in different experiments[12]. The correlation between electron density $n_e$ and azimuthal electric field $E_\theta$, equivalent to a friction force density[10,11]

$$f_{ei} = q\langle n_e E_\theta \rangle \tag{2}$$

between the rotating electrons and almost immobile ions along the azimuthal direction, gives an extra contribution to the electron cross-field mobility (derived by electron momentum conserving equation taking into account azimuthal instabilities[10])

$$\mu_{eff} = \mu_{cl}\left[1 - \frac{\omega_{ce}}{\nu_m}\frac{\langle n_e E_\theta \rangle}{n_{e0}E_{z0}}\right]. \tag{3}$$

where $n_{e0}$ and $E_{z0}$ represent the azimuthally averaged electron density and accelerating axial field, respectively.
This instability has been analyzed in detail by different 1D-azimuthal Particle-in-Cell (PIC)[13,14] models[15-20] assuming fixed axial electric and radial magnetic fields in Cartesian geometry (often used due to the high value of the external diameter to channel with ratio) and using a periodicity length along the azimuthal coordinate always smaller than the real one (Figure 1 represents the corresponding simulation domain). In these models, steady state solutions are reached only if particle losses along the virtual axial boundaries are included. In fact, particles are still tracked along the axial direction (even if their position is not used to self-consistently calculate the axial electric field) and each electron (resp. ion) leaving the simulation domain on the anode (resp. cathode) side is

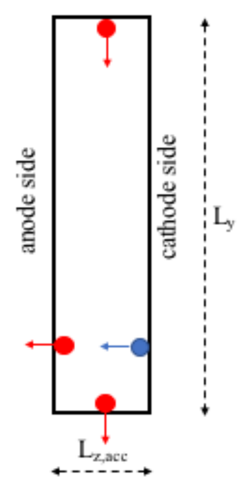


**Figure 1.** *Sketch of the simulation domain used for 1D-azimuthal PIC simulation of Hall thrusters.*

replaced by a new electron (resp. ion) at the cathode (resp. anode) side loaded with an half-Maxwellian velocity distribution with the initial temperature. This particle re-injection mechanism, necessary to avoid undesirable secular effect and to mimic the axial transport, works like an extra collision: reducing the axial-replacement length $L_{z,acc}$ is equivalent to increase the collisional frequency in a 1D-azimuthal model. Usually, the value chosen corresponds to the acceleration region, where both the axial electric and radial magnetic fields can be considered uniform.

All these studies have confirmed a significant fluctuation amplitude of ExB drift instability characterized during the linear stage by high-frequency (of the order of MHz) and discrete number of short-wavelengths (the dominant one of the order of mm) corresponding to cyclotron harmonics

$$\lambda_{ExB\ EDI,m} = \frac{2\pi}{m}\frac{v_{de}}{\omega_{ce}}. \tag{4}$$

where $m$ is an integer. An important feature observed is the difference in the ion and electron density fluctuations. While the electron density perturbation has lower amplitude sinusoidal character, the ion density perturbation is characterized by much larger amplitudes and contains shorter wavelengths (non-quasineutral) with $\lambda \leq \lambda_{De}$ ($\lambda_{De}$ being the electron Debye length) producing highly-localized cnoidal structures with sharper crests and flatter troughs more.

The saturation mechanisms of the instability have been identified in the electron heating, deformation of the electron distribution function projected along the azimuthal direction and ion-wave trapping. The nonlinear stage evolution of the instability instead has given controversial results: some models[17] show a transition of the mode into the regime of the ion-sound instability typical of un-magnetized plasmas, while other models[18] suggest that the magnetic field remains important in the mechanism of the instability, electron heating, and transport. This discrepancy can be attributed to the intrinsic limitation of missing the axial coordinate. In fact, in [17] a re-injection criterion is used while in [18] the particles are kept throughout the simulation as with an infinite acceleration length.

In all the models, the computed cross-field mobility has very large values (one order of magnitude larger) compared with that measured in Hall thrusters. The last point can be related to the fact that the acceleration field $E_{z0}$ is externally imposed and kept fixed, while one expects that an increase of the local mobility would yield a decrease of the local electric field, which would reduce the drift velocity and control the possible instabilities leading to the anomalous electron transport.

Recent models[20-25] have added the radial coordinate resolving the direction along the magnetic field and accounting for the sheath boundary conditions. They have shown that the full ion sound regime is not realized, but a more effective regime of discrete cyclotron resonance instabilities occurs. The magnetic field remains to be a defining feature of ExB drift instability for HT operational regime. On the contrary, the scaling of wavelength, frequency and amplitude of the azimuthal field obtained within azimuthal-axial models[19,26-30] is consistent with the ion acoustic like character of the instability

$$\lambda_{IAI} \approx 2\sqrt{2}\pi\lambda_{De} \tag{5}$$

$$\omega \approx \frac{1}{\sqrt{3}}\omega_{pi} \tag{6}$$

$$|E_\theta| \sim \frac{T_e}{\lambda_{De}}. \tag{7}$$

All the azimuthal models show that results are very sensitive to the numerical parameters used. Instabilities require a very good resolution both in space/time and particle number, in order to have the modes well represented and running up to non-linear and saturation regimes. In particular, numerical noise is responsible for the destruction of electron cyclotron resonance and facilitates the transition to an ion acoustic instability. For this reason, in this work, we have preferred to develop a 1D-azimuthal model by using a high-statistical level. In the next section, the model is explained in detail and the effect of the different re-injection methods is presented. Section III is devoted to the effect of the azimuthal length of the simulation domain on the evolution of the wave spectrum. The scaling of the mobility as a function of plasma density, neutral density, magnetic field, electric field and ion mass has been conducted in Section IV. Finally, the conclusions have been drawn in the last Section V.

## II. Description of the Model and Numerical Convergence Study

The numerical method used is based on electrostatic 1D-azimuthal Particle in Cell / Monte Carlo Collision (PIC-MCC) methodology[13,14]. Uniform radial magnetic $B_0$ and axial electric field $E_{z0}$ are kept fixed during the simulation that starts loading the particles (electrons and ions) uniformly along the azimuthal and axial directions of the simulation domain (represented in Figure 1) and with a prescribed velocity distribution. Electrons and ions are both initialized with a shifted-Maxwellian distribution: electrons at a temperature $T_{e0}$ and with an azimuthal drift $v_{de}=E_{z0}/B_0$, ions with a temperature $T_{i0}$ and an axial drift $v_{id} = \sqrt{2qE_{z0}L_{z,acc}/M}$ ($M$ is the ion mass) corresponding to the velocity acquired by the ions in the acceleration region. Differently from the other components, the axial component of ion velocity is not updated during the simulation and considered as frozen (approximation well posed since ions are treated as collisionless). All the physical parameters used are summarized in Table 1. The cartesian approximation is adopted neglecting the effect of the presence of the centrifugal force. From now on we will use $y$ to represent the azimuthal coordinate $\theta$. The time-step used is $\Delta t = 2x10^{-12}\ s$ . The self-consistent electric field is solved along the ExB direction with a Thomas tridiagonal algorithm modified to implement periodic boundary conditions[31]. The reference zero potential value is put at the boundaries. Electron-neutral collisions (elastic scattering, electronic excitation and ionization) are included. In order to keep the averaged plasma density equal to the initial condition selected, we assume that during the ionization event, only the energy loss and scattering is taken into account, while then new electron-ion pair is not produced. In the present model, we consider the particle re-injection across the axial boundaries. Differently from [17] the re-injected particles are not randomly distributed along the azimuthal direction but they keep their azimuthal positions. They just change their velocity components, exactly like in an inelastic collisional event. This choice is dictated by the fact that, with a random y-location re-injection, a large charge imbalance is artificially created amplified by the fact that the model is one-dimensional. A certain space-charge density (difference between electrons reaching the anode side and ions crossing the cathode one) is created along the ExB direction that generates an artificially high azimuthal electric field. In the 2D-radial-azimuthal extension of the model[25], the random re-injection has much less impact due to the fact that the charge injected is also distributed along the radial dimension. Furthermore, we have verified that results obtained with random azimuthal re-injection are sensitive to the couple of parameters ($L_y$, $L_{z,acc}$) chosen, as already observed in [17]. For small $L_y$ (≤1 cm) or large $L_{z,acc}$ (>2 cm), the reference potential or the low rate of particles re-injected help to keep the azimuthal electric field low.

Figures 2 show the temporal evolution of the averaged (over the particle population) electron (blue curve) and ion (red curve) energy when re-injected particles are loaded with random y-position (a) and when they keep their own azimuthal position had just before the re-injection (b) using $L_y$=2.67 cm and $L_{z,acc}$=1 cm. In the first case, both electron and ion energy increase reaching already after 3 μs unphysical values due to the large azimuthal electric field induced by the random re-injection.

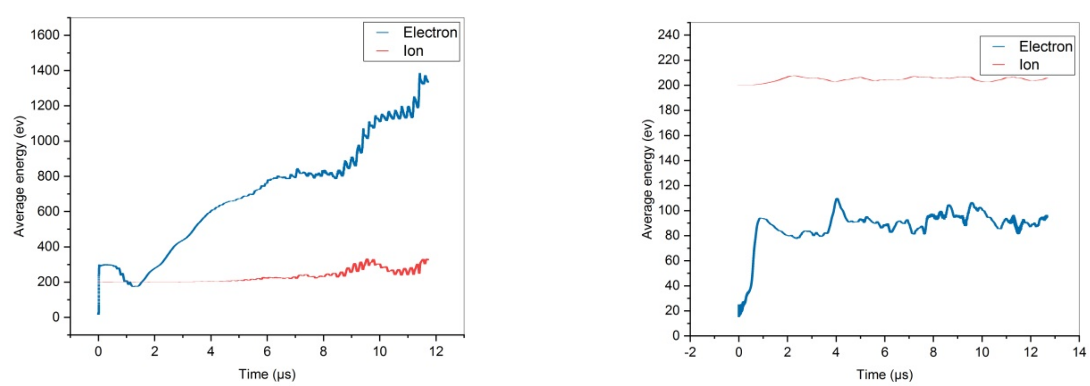


(a) (b)

**Figure 2.** *Averaged electron and ion energy with particle re-injection method across the axial boundaries (a) with random azimuthal positions and (b) preserving azimuthal positions. Results correspond to a case using physical parameters reported in Table 1 (but using an azimuthal simulation domain length of $L_y$=2.67 cm) with number of particles per cell $N_{ppc}$=500 and mesh nodes $N_g$=1000 (corresponding to a cell size of $\boldsymbol{\Delta y = 0.36\lambda_{De}}$).*

Due to the high sensitivity shown by previous models on the numerical parameters used, we have studied the numerical convergence. The global quantities taken as monitoring observables are the electron cross-field mobility and electron density fluctuation level. In case of 1D-azimuthal PIC representation, the mobility can be simply extracted from the averaged axial velocity

$$\mu_{PIC} = \frac{\sum_{ip=1}^{N_p} v_{ip,ez}}{N_p E_{z0}} \tag{8}$$

where $v_{ip,ez}$ is the axial component of the electron velocity and $N_p$ is the total number of particles used in the simulation. The physical condition used are that summarized in Table 1. Figures 3 show a) the electron cross-field mobility and b) the amplitude of fluctuations in electron density computed as a function of number of particles per cell $N_{ppc}$ (from 20 to 1000) for four different numbers of mesh nodes, $N_g$=250, 500, 1000 and 2000, corresponding to four different values of cell size to Debye length ratio $\frac{\Delta y}{\lambda_D}$=1.44, 0.72, 0.36 and 0.18. Results correspond to a time larger than 10 $\mu s$ and the mobility and fluctuation amplitude reported were also time averaged over the last 2 µs. For $N_{ppc}$>500 all the cases give results close to the averaged value of $\mu_{PIC}$=3.4 m$^2$V$^{-1}$s$^{-1}$ within a deviation less than 5% and fluctuations in the electron density around 22% of the equilibrium density. The electron heating growth rate does not change if using $N_{ppc}$ larger than 500 and $N_g$ larger than 1000. Therefore, for the rest of the work, we have fixed the numerical parameters at $N_{ppc}$=500 and $\frac{\Delta y}{\lambda_D}$=0.36.

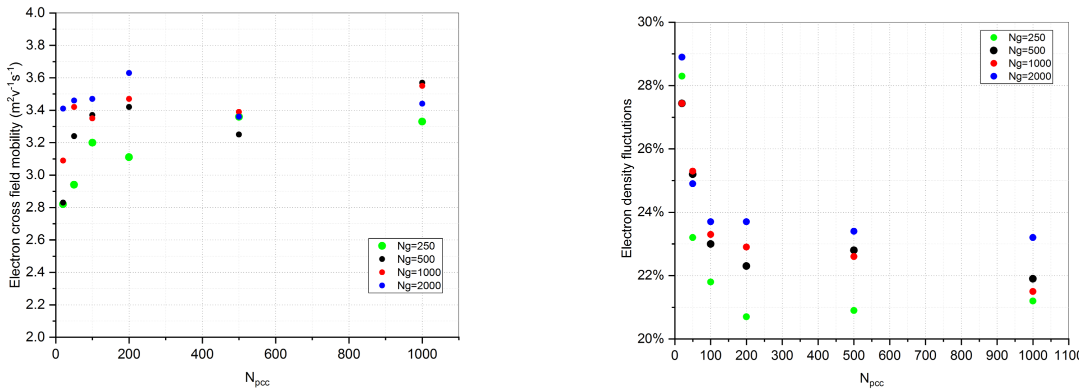


(a) (b)

**Figure 3.** *a) Computed mobility using Eq. (7) and b) amplitude of fluctuations in electron density as a function of the number of particles per cell $N_{ppc}$ for four different cell size $\frac{\Delta y}{\lambda_{De}}$=1.44 (number of mesh nodes $N_g$=250), 0.72 ($N_g$=500), 0.36 ($N_g$=1000) and 0.18 ($N_g$=2000). All the cases correspond to physical parameters reported in Table 1 using azimuthal length of $L_y$=2.67 cm.*

## III. Reference Case

In this section we present results obtained using physical data reported in Table 1. It is considered as reference case for the physical parametrical scan study reported in the next Sect. IV.

Table 1 – Physical parameter used in the test case.

| Physical Parameter | Value | Derived Quantity | Value |
|---|---|---|---|
| $L_y$ (cm) | 5.34 | Electron Plasma frequency $\omega_{pe}$ (rad s$^{-1}$) | 1.79x10$^{10}$ |
| $L_{z,acc}$ (cm) | 1 | Ion Plasma frequency $\omega_{pi}$ (rad s$^{-1}$) | 3.64x10$^7$ |
| $n_{p0}$ (m$^{-3}$) | 1x10$^{17}$ | Electron cyclotron frequency $\omega_{ce}$ (rad s$^{-1}$) | 3.56x10$^9$ |
| Ion species | Xe | Electron-gas collisional frequency $\nu_m$ (s$^{-1}$) | 1.32x10$^6$ |
| $n_N$ (m$^{-3}$) | 2x10$^{18}$ | Debye length $\lambda_{De}$ (m) | 7.43x10$^{-5}$ |
| $B_0$ (G) | 200 | Electron gyroradius $\rho_e$ (m) | 5.98x10$^{-4}$ |
| $E_{z0}$ (Vcm$^{-1}$) | 200 | First cyclotron harmonic wavelength $\lambda_1$ (m) | 1.76x10$^{-3}$ |
| $T_{e0}$ (eV) | 10 | Electron thermal velocity $v_{th,e}$ (m s$^{-1}$) | 2.12x10$^6$ |
| $T_{i0}$ (eV) | 0.2 | Electron ExB drift $v_{de}$ (m s$^{-1}$) | 1.00x10$^6$ |
| $T_N$ (K) | 700 | Hall parameter $\beta$ | 2.70x10$^3$ |

Figure 4 shows an overview of the simulation run. The history of the global averaged electron / ion energy and electrostatic potential energy density $u_E = \frac{1}{2}\varepsilon_0 E_y^2$ are displayed over a total time of 5 µs. In the graph one can identify four stages: 1) the linear growth, a very fast process terminating already after the first microsecond; 2) the first nonlinear stage ending at $t$=3.5 µs and during which the electron energy appears to saturate; this phase corresponds to a redistribution of the spectral energy towards lower harmonics (see Figure 6.b) and to the ion heating; 3) the second nonlinear phase when the electron and ion energy rise again; 4) the final quasi-steady state reached after $t$=4.5 μs.

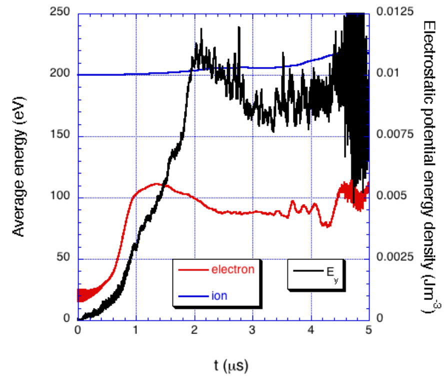


**Figure 4.** *Electron (red curve), ion (blue curve) averaged energy and electrostatic potential energy density (black curve) in the simulation up to t=5 μs. Results refer to the reference case using physical parameters reported in Table 1.*

Figures 5 show a) the time evolution of the azimuthal profile of $E_y$ and b) the time evolution of the corresponding power spectral density (PSD) into wavenumber $k_y$ components. The instability starts during the linear stage (for $t$<2 μs) with the growth of the most instable cyclotron harmonics (seven different harmonics are easily distinguishable from the spectrum) whose dominant one has the following characteristics: wavelength k=3650 m$^{-1}$ (corresponding to the first cyclotron harmonic $m$=1 of Eq. (4)), frequency $\omega$=4.8 MHz and phase velocity $v_\varphi$=8 km/s in the ExB drift direction. However, the values found are also in good agreement with Eq. (5), the theoretical estimation of an ion acoustic character found in Ref. [11] using the wavenumber with the maximum growth. Using an electron temperature of $T_e$=60 eV (computed in the non-linear phase) Eq. (5) gives $k_{IAI}$=3890 m$^{-1}$, while Eq. (6) gives $\omega$ =3.2 MHz. For $t$>2 μs, the highest cyclotronic harmonics are strongly attenuated. The resonance character of the ExB EDI based on the linear treatment and Maxwellian behavior of electron distribution function, disappears by a resonance broadening mechanism[32]. Only the first harmonic remains detectable making the electrons still keeping their magnetization even if much weaker. Furthermore, a very low $k$-number component (much lower than the fundamental cyclotron mode $k_1$) appears corresponding to wavelengths comparable to the entire simulation domain size. Already previous 1D-azimuthal and 2D-radial-azimuthal models[18,23,25] have shown nonlinear development of large-scale modes, comparable to the entire azimuthal size of the simulation domain. Finally, the instability is observed to stabilize when the amplitude is large enough to trap a significant portion of ions: the confirmation comes from the ion heating and rotation since the free energy dissipates by giving the ion distribution a long tail, rather than driving exponentially growing azimuthal electric field.

(a)
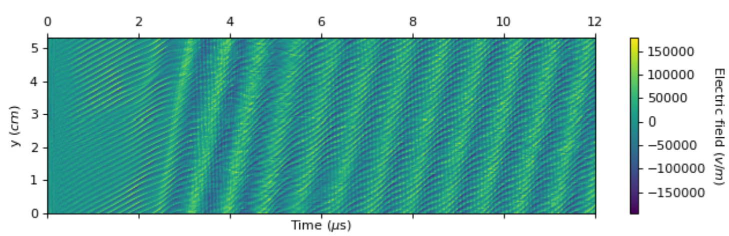


(b)
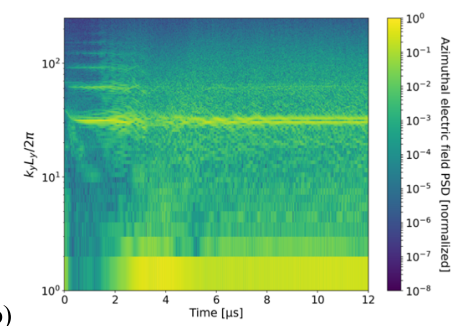


**Figure 5.** *a) Temporal evolution of a) the azimuthal profile of the oscillating electric field $E_y$ and of b) the corresponding distribution of power spectral density into wavenumber components $S_{Ey}(k_y)$.*

## IV. Parametrical study and scaling laws

Since operating parameters (Table 1) are very effective on the ExB EDI and as a consequence, on the global electron cross-field transport, we are interesting to conduct a study of the behavior of the electron cross-field mobility (calculated following Eq. (8)) as a function of the most important input data used: neutral density, plasma density, magnetic field, accelerating electric field and ion mass. In addition, the total cross-field mobility derived by electron momentum conserving equation taking into account azimuthal instabilities, Eq. (3), is also used for comparison. The azimuthal correlation between the electron density and azimuthal electric field is computed in the PIC model through a double integral formula by using a time-averaged (over an interval $T$=2 μs) value

$$\langle n_e E_y \rangle = \int_0^{Ly} \int_0^{T} \frac{dy}{Ly}\frac{dt}{T} n_e(y,t) E_y(y,t) \tag{10}$$

discretized using the Simpson's 1/3 rule[33].

Figure 6.a shows the gas density dependence keeping the other physical parameters fixed to the values reported in Tab. 1. This study allows knowing the effect of collisions on the mobility since the contribution of instability does not depend on the electron-neutral collisional frequency. At very low gas density, the contribution to the electron cross-field mobility predominantly comes from the instability: its initial value is mostly determined by the second term on the right-hand side of Eq. (5). However, we must remember that the particle re-injection technique adopted (see Sect. II) corresponds to an artificial collision always present even in the case of very low gas density. As the gas density increases the collisional contribution becomes stronger (mixed regime) and the cross-field mobility increases reaching its maximum for $n_N$=8x10$^{20}$ m$^{-3}$. For much larger gas density the regime is collision-dominated (the first term on the right-hand side of Eq. (5) is dominant): the mobility change behavior decreasing as the gas density increases following the classical collisional dependence Eq. (1) (for $\nu_m \gg \omega_{ce}$) $\mu_\perp \propto \frac{1}{n_N}$.

Figure 6.b shows the electron cross-field mobility as a function of the magnetic field imposed. Both estimations follows the classical behavior Eq. (1) $\mu_\perp \propto \frac{1}{B^2}$ (green curve), but the effective collisional frequency $\nu_{m,eff}$ results 50 times larger than the real value reported in Table 1. This proofs that in Hall thruster regime, the electron ExB drift instability does not induce full turbulence Bohm-like behavior $\mu_{\perp,Bohm} \propto \frac{1}{B}$.

Figure 6.c shows the electron cross-field mobility as a function of the plasma density studying the pure effect of the instability on the electron transport (the gas density is kept fixed to $n_N$=2x10$^{18}$ m$^{-3}$). In agreement with values found by previous PIC simulations[16,17], the mobility always increases with the plasma density starting from the pure collisional value assumed at very low plasma density (no instability) given by Eq. (1) $\mu_\perp = 1.8x10^{-2}\ m^2V^{-1}s^{-1}$.

In Figure 6.d the behavior of the electron mobility as a function of the applied axial electric field is reported. A larger $E_{z0}$ gives larger ExB drift and therefore stronger electron cyclotron instability. As a consequence, the mobility shows a continuous growth in the range analyzed.

Figure 6.e reports the effect of the ion mass, where the most relevant noble gases (He, Ne, Ar, Kr and Xe) have been used. The different cases all use the same cross section in order to avoid possible contamination on the mobility

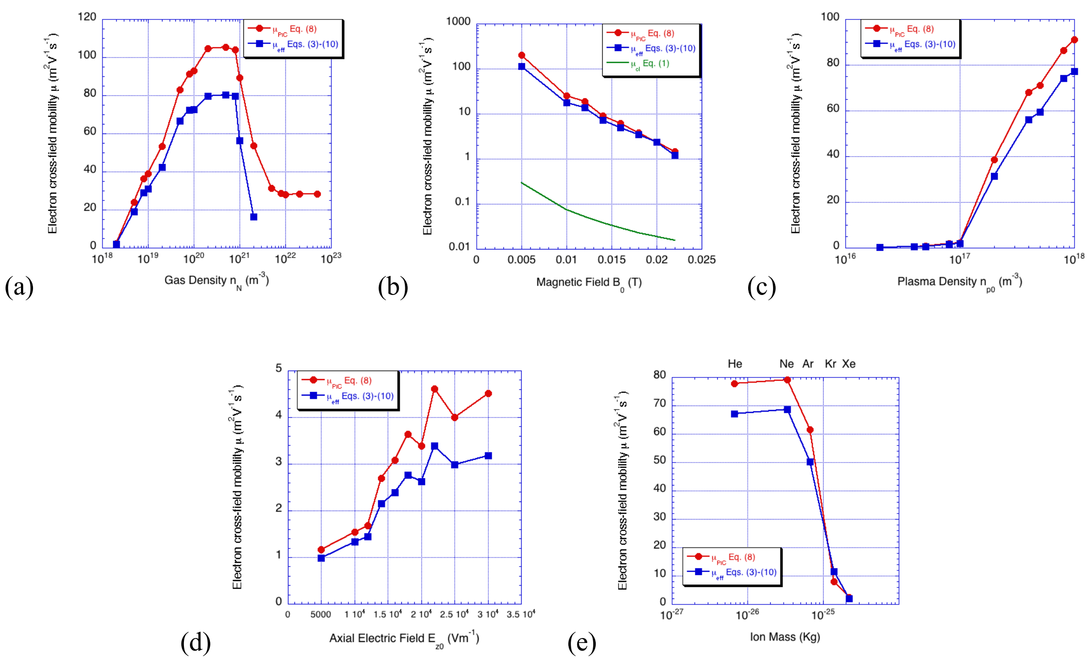


**Figure 6.** *Calculated steady state cross-field mobility as a function of (a) xenon gas density, (b) magnetic field, (c) plasma density, (d) axial electric field and (e) ion mass, using data reported in Table 1.*

due to the different cross sections, and measure in this way the pure ion mass effect. As evident, heavier ions lead to a strong reduction (larger than 10 times) of the electron cross-field mobility. The behavior is in agreement with the kinetic theoretical treatment of [11] that have shown as the onset conditions for instability are reduced and the unstable region is broader for lighter ions.

## V. Conclusions

In this work, we have presented a numerical study, based on 1D Particle-in-Cell methodology, of the electron ExB drift instability in Hall thruster. It gives correlated fluctuations in electron density and electric field leading to enhanced electron cross-field mobility. The local representation is simplified since it neglects any effects of axial gradients, radial contributions and assumes a constant axial electric field. Nevertheless, the description allows having a high statistical level, condition necessary to reduce the effect of numerical heating on the linear and non-linear evolution and on saturation of the instability.

Results show that the fluctuation spectra remain quantized (electron magnetization signature) predominantly retaining the fundamental cyclotron mode. In addition, using larger azimuthal simulation domains (forcing the periodicity length towards a realistic value), the development of long wavelength envelope comparable to the entire azimuthal extension, appears.

An accurate parametrical study has also been conducted to find the behavior of electron cross-field mobility as a function of the most important operative quantities: gas and plasma density, magnetic field, axial electric field and ion mass. The electron cross-field transport shows a strong dependence on the plasma density and ion mass. The computed dominant wavelength scales according to the ExB EDI and no transition towards ion acoustic like instability is observed.

## References

[1]Zhurin, V. V., Kaufman, H. R., and Robinson, R. S., Physics of closed drift thrusters, *Plasma Sources Sci. Technol.*, Vol. 8, 1999, pp. R1.

[2]Morozov A. I., and Savelyev, V. V. *Fundamentals of stationary plasma Thruster theory*. *In: Kadomtsev B.B., Shafranov V.D. (eds) Reviews of Plasma Physics. Reviews of Plasma Physics*, vol 21. Springer, Boston, MA, 2000.

[3]Goebel, D. M., and Katz, I., *Fundamentals of electric propulsion: Hall and ion thrusters*, John Wiley & Sons, Hoboken, 2008.

[4]Boeuf, J. P., "Physics and modeling of Hall thrusters," *J. Appl. Phys.*, Vol. 121, 2017, 011101.

[5]Morozov, A. I., and Savelyev, V. V., "Theory of the near-wall Conductivity," *Plasma Phys. Rep.*, Vol. 27, 2001, pp. 570.

[6]Janes, G. S., and Lowder, R. S., "Anomalous electron diffusion and ion acceleration in a low-density plasma," *Phys. Fluids*, Vol. 9, 1966, pp. 1115.

[7]Scharfe, M. K., Thomas, C. A., Scharfe, D. B., Gascon, N., Cappelli, M. A., and Fernandez, E., "Shear-based model for electron transport in hybrid Hall thruster simulations," *IEEE Trans. Plasma Science*, Vol. 36, 2008, pp. 2058.

[8]Cappelli, M. A., Young, C. V., Cha, A., and Fernandez, E., "A zero-equation turbulence model for two-dimensional hybrid Hall thruster simulations," *Phys. Plasmas*, Vol. 22, 2015, 114505.

9Jorns, B., "Predictive, data-driven model for the anomalous electron collision frequency in a Hall effect thruster," *Plasma Sources Sci. Technol.*, Vol. 27, 2018, 104007.

[10]Lafleur, T., Baalrud, S. D., and Chabert, P., "Theory for the anomalous electron transport in Hall effect thrusters. II. Kinetic model," *Phys. Plasmas*, Vol. 23, 2016, 053503.

[11]Lafleur, T., Baalrud, S. D., and Chabert, P., "Characteristics and transport effects of the electron drift instability in Hall-effect thrusters," *Plasma Sources Sci. Technol.*, Vol. 26, 2017, 024008.

[12]Tsikata, S., Honoré, C., Lemoine, N., and Grésillon, D. M., "Three-dimensional structure of electron density fluctuations in the Hall thruster plasma: ExB mode," *Phys. Plasmas*, Vol. 17, 2010, 112110 (2010).

[13]Hockney, R. W., and Eastwood, J. W., *Computer simulation using particles*, IOP Publishing Ltd, 1989.

[14]Birdsall, C. K., and Langdon, A. B., *Plasma physics via computer simulation*, Taylor and Francis, 2005.

[15]Ducrocq, A., Adam, J. C., Héron, A., and Laval, G., "High-frequency electron drift instability in the cross-field configuration of Hall thrusters," *Phys. Plasmas*, Vol. 13, 2006, 102111.

[16]Boeuf, J. P., "Rotating structures in low temperature magnetized plasmas—insight from particle simulations," *Front. Phys.*, Vol. 2, 2014, pp. 74.

[17]Lafleur, T., Baalrud, S. D., and Chabert, P., "Theory for the anomalous electron transport in Hall effect thrusters. I. Insights from particle-in-cell simulations," *Phys. Plasmas*, Vol. 23, 2016, 053502.

[18]Janhunen, S., Smolyakov, A., Chapurin, O., Sydorenko, D., Kaganovich, I., and Raitses, Y., "Nonlinear structures and anomalous transport in partially magnetized ExB plasmas," *Phys. Plasmas*, Vol. 25, 2018, 011608.

[19]Katz, I., Chaplin, H., Lopez Ortega, A., "Particle-in-cell simulations of Hall thruster acceleration and near plume regions," *Phys. Plasmas*, Vol. 25, 2018, 123504.

[20]Hara, K., "An overview of discharge plasma modeling for Hall effect thrusters," *Plasma Sources Sci. Technol.*, Vol. 28, 2019, 044001.

[21]Héron, A., and Adam, J. C., "Anomalous conductivity in Hall thrusters: Effects of the non-linear coupling of the electron-cyclotron drift instability with secondary electron emission of the walls," *Phys. Plasmas*, Vol. 20, 2013, 082313.

[22]Croes, V., Lafleur, T., Bonaventura, Z., Bourdon, A., and Chabert, P., "2D particle-in-cell simulations of the electron drift instability and associated anomalous electron transport in Hall-effect thrusters," *Plasma Sources Sci. Technol.*, Vol 26, 2017, 034001.

[23]Janhunen, S., Smolyakov, A., Sydorenko, D., Jimenez, M., Kaganovich, I., and Raitses, Y., Evolution of the electron cyclotron drift instability in two-dimensions, *Phys. Plasmas*, Vol. 25, 2018, 082308.

[24]Tavant, A., Croes, V., Lucken, R., Lafleur, T., Bourdon, A., and Chabert, P., The effects of secondary electron emission on plasma sheath characteristics and electron transport in an ExB discharge via kinetic simulations, *Plasma Sources Sci. Technol.*, Vol. 27, 2018, 124001.

[25]Taccogna, F., Minelli, P., Asadi, Z., and Bogopolsky, G., "Numerical studies of the ExB electron drift instability in Hall thrusters", *Plasma Sources Sci. Technol.*, Vol. 28, 2019, 064002.

[26]Adam, J. C., Héron, A., and Laval, G., "Study of stationary plasma thrusters using two-dimensional fully kinetic simulations," Phys. Plasmas, Vol. 11, 2004, pp. 295.

[27]Coche, P., and Garrigues, L., "A two-dimensional (azimuthal-axial) particle-in-cell model of a Hall thruster," *Phys. Plasmas*, Vol. 21, 2014, 023503.

[28]Lafleur, T., and Chabert, P., "The role of instability-enhanced friction on 'anomalous' electron and ion transport in Hall-effect thrusters," *Plasma Sources Sci. Technol.*, Vol. 27, 2018, 015003.

[29]Lafleur, T., Martorelli, R., Chabert, P., and Bourdon, A., "Anomalous electron transport in Hall-effect thrusters: Comparison between quasi- linear kinetic theory and particle-in-cell simulations," *Phys. Plasmas*, Vol. 25, 2018, 061202.

[30]Boeuf, J. P., and Garrigues, L. "ExB electron drift instability in Hall thrusters: Particle-in-cell simulations vs. theory," *Phys. Plasmas,* Vol. 25, 2018, 061204.

[31]Napolitano, M., "A FORTRAN subroutine for the solution of periodic block-tridiagonal systems," *Comm. Appl. Num. Meth.*, Vol. 1, 1985, pp. 11-15.

[32]Muschietti, L, and Lembège, B., "Microturbulence in the electron cyclotron frequency range at perpendicular supercritical shocks," *J. Geophys. Res.: Space Phys.*, Vol. 118, 2013, pp. 2267.

[33]Sadiku, M. N. O., *Numerical techniques in electromagnetics*, 2$^{nd}$ edition, CRC Press, Boca Raton, 2001.